Langmuir
Article
pubs.acs.org/Langmuir

Surface Composition, Chemistry, and Structure of Polystyrene Modified by Electron-Beam-Generated Plasma

Evgeniya H. Lock,*,† Dmitri Y. Petrovykh,‡,§ Paul Mack,∥ Tim Carney,∥ Richard G. White,∥ Scott G. Walton,† and Richard F. Fernsler†

†*Plasma Physics Division, and* ‡*Chemistry Division, Naval Research Laboratory, Washington, D.C. 20375,* §*Department of Physics, University of Maryland, College Park, Maryland 20742, and* ∥*Thermo Fisher Scientific, The Birches Industrial Estate, Imberhorne Lane, East Grinstead, West Sussex RH19 1UB, United Kingdom*

Received December 8, 2009. Revised Manuscript Received March 15, 2010

Polystyrene (PS) surfaces were treated by electron-beam-generated plasmas in argon/oxygen, argon/nitrogen, and argon/sulfur hexafluoride environments. The resulting modifications of the polymer surface energy, morphology, and chemical composition were analyzed by a suite of complementary analytical techniques: contact angle goniometry, atomic force microscopy (AFM), X-ray photoelectron spectroscopy (XPS), and reflection electron energy loss spectroscopy (REELS). The plasma treatments produced only minimal increases in the surface roughness while introducing the expected chemical modifications: oxygen-based after Ar/O_2 plasma, oxygen- and nitrogen-based after Ar/N_2 plasma, and fluorine-based after Ar/SF_6 plasma. Fluorinated PS surfaces became hydrophobic and did not significantly change their properties over time. In contrast, polymer treated in Ar/O_2 and Ar/N_2 plasmas initially became hydrophilic but underwent hydrophobic recovery after 28 days of aging. The aromatic carbon chemistry in the top 1 nm of these aged surfaces clearly indicated that the hydrophobic recovery was produced by reorientation/diffusion of undamaged aromatic polymer fragments from the bulk rather than by contamination. Nondestructive depth profiles of aged plasma-treated PS films were reconstructed from parallel angle-resolved XPS (ARXPS) measurements using a maximum-entropy algorithm. The salient features of reconstructed profiles were confirmed by sputter profiles obtained with 200 eV Ar ions. Both types of depth profiles showed that the electron-beam-generated plasma modifications are confined to the topmost 3−4 nm of the polymer surface, while valence band measurements and unsaturated carbon signatures in ARXPS and REELS data indicated that much of the PS structure was preserved below 9 nm.

1. Introduction

A combination of versatile physical and chemical properties and low cost makes polymers ideal candidates for diverse applications, including organic and flexible electronics, platforms for biological research, and biomedical devices and materials.[1−3] For example, the polymer analyzed in this work, polystyrene (PS), has conduction characteristics and dielectric strength that make it a promising insulator for organic electronics applications.[4] For biomedical applications, polystyrene has been successfully used as a platform for bioanalytical assays, as a hemocompatible material, in antimicrobial surfaces, and in tissue engineering.[5] However, like most polymers, polystyrene is chemically inert and thus needs to be functionalized for applications that require increased wettability, adhesion, or covalent immobilization of chemical and biological ligands. These desirable properties have been successfully produced by plasma treatments of polymer surfaces.[6−10] Furthermore, plasma-induced polymer cross-linking results in increase in hardness and wear resistance. However, energetic plasmas should be used with caution because they can produce surface roughening and modification depths that are too large for some surface-sensitive nanometer scale applications. Plasmas are typically created by applying electric fields to energize the plasma electrons. These energetic electrons interact with the background gas via electron-driven ionization and dissociation reactions producing ions, radicals, and excited species, which ultimately transform the polymer surface. The production of excited species will generate UV and VUV photons that penetrate up to a few micrometers into the polymer and produce chemical and morphological modifications of the polymer surface.[11] The fundamental plasma characteristics, for example, electron temperature and plasma density, are controlled by the source type and operating conditions. Discharges used for material processing typically have densities of 10^9-10^{12} cm^{-3} and electron temperatures (T_e) in the range of 1−10 eV. The electron temperature determines the plasma potential and thus establishes the minimum ion energy at surfaces located adjacent to the plasma. The incident ion energy strongly influences the particular material processing application, which can range from sputtering to cross-linking. However, for treatment of sensitive materials, such as polymers, high incident ion energy

*To whom correspondence should be addressed. Telephone: 202-767-0351. Fax: 202-767-3553. E-mail: evgeniya.lock@nrl.navy.mil.

(1) Lee, D. Y.; Hines, D. R.; Stafford, C. M.; Soles, C. L.; Lin, E. K.; Oehrlein, G. S. *Adv. Mater.* **2009**, *21*, 2524–2529.
(2) Favia, P.; Sardella, E.; Gristina, R.; d'Agostino, R. *Surf. Coat. Technol.* **2003**, *169*, 707–711.
(3) Liqiang, C.; Wolfgang, K.; Renate, F. *Plasma Processes Polym.* **2006**, 498–505.
(4) Prime, D.; Paul, S.; Josephs-Franks, P. W. *IEEE Trans. Dielectr. Electr. Insul.* **2008**, *15*, 905–909.
(5) Goddard, J. M.; Hotchkiss, J. H. *Prog. Polym. Sci.* **2007**, *32*, 698–725.
(6) Grace, J. M.; Gerenser, L. J. *J. Dispersion Sci. Technol.* **2003**, *24*, 305–341.
(7) Shi, M. K.; Selmani, A.; Martinu, L.; Sacher, E.; Wertheimer, M. R.; Yelon, A. *J. Adhes. Sci. Technol.* **1994**, *8*, 1129–1141.
(8) Hegemann, D.; Brunner, H.; Oehr, C. *Nucl. Instrum. Methods Phys. Res., Sect. B* **2003**, *208*, 281–286.
(9) Garrison, M. D.; Luginbuhl, R.; Overney, R. M.; Ratner, B. D. *Thin Solid Films* **1999**, *352*, 13–21.
(10) Lopez, L. C.; Gristina, R.; Ceccone, G.; Rossi, F.; Favia, P.; d'Agostino, R. *Surf. Coat. Technol.* **2005**, *200*, 1000–1004.
(11) Kreutz, E. W.; Frerichs, H.; Stricker, J.; Wesner, D. A. *Nucl. Instrum. Methods Phys. Res., Sect. B* **1995**, *105*, 245–249.

promotes undesirable surface roughening and even damage to the polymer surfaces.[12]

In contrast, polystyrene films in this study were modified by *electron-beam-generated plasmas* that are characterized by low electron temperatures, by low plasma potentials, and by correspondingly low incident ion energies.[13] Furthermore, nearly half of the energy deposited by the beam goes directly into ionization, thus limiting the relative concentration of excitation and dissociation products as well as generation of UV and VUV photons. The produced high ion fluxes ensure that the *surface chemistry* of the polymers is efficiently modified. On the other hand, the low ion energies limit the undesirable physical sputtering and ion-assisted chemical etching of polymer surfaces. Thus, electron-beam-generated plasmas cause limited changes to the polymer *surface morphology* and result in low total *depth of modification*. More broadly, these characteristics make electron-beam plasmas ideal for treating a range of soft and/or very thin materials, particularly when nanometer-scale features are critical.

To better quantify the modification of polymers exposed to electron-beam plasmas, polystyrene surfaces were treated in Ar/N_2, Ar/O_2, and Ar/SF_6 environments and then characterized using a suite of complementary analytical techniques, including contact angle goniometry, atomic force microscopy (AFM), and X-ray photoelectron spectroscopy (XPS). The most critical properties, surface chemistry and depth of modification, were determined from a series of XPS measurements that probed chemical composition at progressively shallower sampling depths. Valence band (VB) spectroscopy probed the polystyrene films down to ca. 12 nm below the surface, which can be considered as "bulklike" depth for plasma-treated polymers. Parallel angle-resolved XPS (ARXPS) measurements were used to reconstruct nondestructive depth profiles in the 1−6 nm range, where the chemical modification is expected to occur for beam-produced plasmas. The salient features of these nondestructive depth profiles were confirmed by low energy Ar sputter depth profiling. In addition, carbon chemistry of the topmost 0.5−1.5 nm of polystyrene was verified by reflection electron energy loss spectroscopy (REELS).

2. Materials and Methods

2.1. Polystyrene Film Preparation. Polystyrene (Sigma Aldrich, ca. 280 000 MW by GPC) supplied in pellet form was dissolved and spin-coated on top of 300 μm thick, prime-grade silicon wafers (Silicon Quest, Inc.).[14] Pellets of amorphous polystyrene dissolve readily in organic solvents; toluene (anhydrous 99.8%, Sigma Aldrich) was chosen in this study. Heating of the polystyrene solution in toluene (2 wt %) to 50 °C for 2 h was sufficient to completely dissolve the solid polymer. The films were spin-coated at 3000 rpm for 1 min. The thickness of the resulting polymer films was ca. 100 nm, with sample-to-sample variation of < 5 nm. After preparation, films were placed in a desiccator for 24 h to ensure complete solvent evaporation.

2.2. Plasma System and Polystyrene Film Treatment. The experimental apparatus has been discussed previously.[15] The system vacuum was maintained by using a 250 L/s turbo pump, with a base pressure of 5×10^{-6} Torr. The operating pressure was achieved by introducing Ar (purity >99.9999%), O_2 (purity >99.999%), N_2 (purity >99.999%), and SF_6 (purity >99.999%) through mass flow controllers and by throttling the pumping speed using a manual gate valve. The electron beam was produced by applying a −2 kV pulse to a linear hollow cathode for a selected pulse width and duty factor. The emergent beam passed through a slot in a grounded anode and was then terminated at a second grounded anode located further downstream. The electron beam volume between the two anodes defines the ionization source volume, with the dimensions set by the slot size (1×25 cm^2) and the anode-to-anode length (40 cm). Beam spreading from collisions with the background gas was suppressed by a coaxial magnetic field (150 G) produced by a set of external coils. Because the beam is collimated, few high energy electrons strike the surface of the material. The samples were placed on a 10.2 cm diameter stage located at 2.5 cm from the nominal edge of the electron beam. The stage was held at ground potential and room temperature.

All of the treatments were conducted at a pressure of 50 mTorr. The total gas flow rate was held constant at 50 sccm, and the flow of oxygen and nitrogen gases in argon/oxygen (Ar/O_2) and argon/nitrogen (Ar/N_2) mixtures was 10% (5 sccm of oxygen or nitrogen, respectively). The flow of SF_6 in Ar/SF_6 mixture was 5% (2.5 sccm of SF_6). The exposure times for Ar/N_2 and Ar/O_2 were 30 s, whereas for Ar/SF_6 the exposure was 60 s. The plasma period was 20 ms, and the duty factor was 10%. The period is defined as the time between two consecutive pulses, comprising the beam pulse width (when plasma is produced), the afterglow (when plasma decays), and the time when no plasma is present; the duty factor is defined as the ratio of the plasma on-time to the period. Thus, for total treatment times of 5 and 10 min, the nominal plasma exposure times were 30 and 60 s, respectively.

2.3. Atomic Force Microscopy. The polymer surface morphology was examined at various scales using an atomic force microscope (Nanoscope III, Veeco Metrology, Santa Barbara, CA) operated in tapping mode. Surface images for quantitative analysis were obtained from 1×1 μm^2 scans at a resolution of 256×256 pixels and scan rate of 1.5 Hz.

2.4. Contact Angle Goniometry and Surface Energy Estimation. Contact angle measurements were performed with an automated goniometer (AST Products, Inc.). Drops of selected liquids with known surface tension (water, ethylene glycol, and diiodomethane) were positioned on the surface with microsyringes designated for a particular liquid. The contact angles of both sides of three 2 μL drops were averaged for each sample. The surface energy was estimated using the Wendt−Owens model.[16]

2.5. XPS and REELS Measurements. *2.5.1. Valence Band(VB) Spectroscopy*. Spectra in the VB fingerprint region were acquired in a commercial K-Alpha instrument (Thermo Fisher Scientific, Inc.) with excitation from a microfocused Al Kα X-ray source, which illuminated a spot of 400×600 μm^2 on the sample. In K-Alpha instruments, the energy of the monochromated Al Kα X-ray source is automatically calibrated and maintained at 1486.6 ± 0.2 eV. The VB data were recorded from 0 to 40 eV binding energy (BE) with the analyzer pass energy set to 50 eV (corresponding to energy resolution of ca. 0.7 eV). Spatially uniform charge neutralization in a K-Alpha instrument is provided by a dedicated system that directs beams of low energy (≤10 eV) electrons and Ar ions onto the sample. Charge compensation was verified by observing the main C 1s peak at BE = 285.0 eV.

2.5.2. Parallel Angle-Resolved XPS. A commercial Theta Probe instrument (Thermo Fisher Scientific, Inc.) with parallel detection capability was used to acquire surveys and element-specific high-resolution spectra simultaneously over a 60° range of emission angles. A microfocused monochromated Al Kα X-ray source was set to illuminate a spot of 400 μm in size. Parallel ARXPS data were acquired with analyzer pass energy set to 100 eV. Photoelectron signal from the two-dimensional

(12) Strobel, M.; Dunatov, C.; Strobel, J. M.; Lyons, C. S.; Perron, S. J.; Morgen, M. C. *J. Adhes. Sci. Technol.* **1989**, *3*, 321–335.
(13) Walton, S. G.; Muratore, C.; Leonhardt, D.; Fernsler, R. F.; Blackwell, D. D.; Meger, R. A. *Surf. Coat. Technol.* **2004**, *186*, 40–46.
(14) Lock, E. H.; Walton, S. G.; Fernsler, R. F. *Preparation of ultra thin polystyrene, polypropylene and polyethylene films on Si substrate using spin coating technology*, NRL/MR/6750-08-9092, **2008**.
(15) Leonhardt, D.; Muratore, C.; Walton, S. G. *IEEE Trans. Plasma Sci.* **2005**, *33*, 783–790.
(16) Owens, D. K.; Wendt, R. C. *J. Appl. Polym. Sci.* **1969**, *13*, 1741–&.

detector was binned into 16 emission angle channels uniformly distributed between 21.875° and 78.125°. Using this method, 16 angle-resolved spectra per elemental region were acquired *simultaneously*, without tilting the sample. Charge compensation and BE referencing procedures were similar to those described in section 2.5.1.

2.5.3. XPS Peak Fitting and Quantification. High-resolution elemental spectra were fit using two commercial XPS analysis software packages: Unifit[17] and Avantage (version 4.31, Thermo Fisher Scientific). A convolution of Gaussian and Lorentzian line shapes was assumed for individual peaks, following the line shape parametrization for polystyrene established in previous high-resolution XPS study.[18] To produce consistent fits of minor C 1s components, which are superimposed on the inelastic background of the main peak, a linear combination of Shirley and linear functions with consistent parameters was used to model the background. Multiple-component fitting in the C 1s region always started from the lowest BE component, and its full-width at half-maximum (fwhm) was used to constrain the fwhm's for the other components. The standard "atomic %" elemental compositions were quantified using calibrated analyzer transmission functions, Scofield sensitivity factors,[19] and effective attenuation lengths (EALs) for photoelectrons; EALs were calculated using the standard TPP-2M formalism[20,21] (see section 2.5.5 for details).

2.5.4. Reflection Electron Energy Loss Spectroscopy. The aromaticity of carbon in the topmost layers of polystyrene films was investigated by angle-resolved REELS measurements in a Theta Probe instrument. The incident monokinetic electron beams for REELS experiments were produced by an electron flood source set to a beam current of 2 μA and energies of 250 or 500 eV. The analyzer pass energy was set to 50 eV, and angle-resolved spectra of reflected electrons were scanned from 100 eV below the primary beam energy toward the elastic peak.

2.5.5. Effective Attenuation Length Calculations. The XPS and ARXPS data were analyzed following the standard formalism based on the assumption that detected electrons are exponentially attenuated when passing through the analyzed material.[20,22] The corresponding EAL for photoelectrons (often denoted as λ in XPS formulas) sets the scale for estimating the sampling depth of the analysis and for determining elemental depth profiles. In the following discussion, the XPS (and REELS) sampling depth is defined as 3λ, which is a common practical definition because ca. 95% of the signal is derived from the corresponding analysis region.[23] In the ARXPS analysis, EAL values are modified by the cosine of the respective detection angle.[20,22,24,25]

The EAL values in Table 1 have been calculated using the standard TPP-2M formalism, based on the kinetic energy of the detected electrons.[20,21] In addition to standard coefficients tabulated for main photoelectron peaks, the TPP-2M formula includes material parameters, which for the PS samples in this work were assumed to be close to bulk values for typical high-density homopolymers: density of 1.0 g/cm^3 and band gap of 5 eV. Small changes in these material parameters do not affect the EAL calculations significantly.[26]

2.6. Quantitative Depth Profiles. *2.6.1. Nondestructive Depth Profiles*. The nondestructive elemental depth profiles were reconstructed from parallel ARXPS data using an iterative maximum-entropy algorithm[24,25] implemented in Avantage software (version 4.31, Thermo Fisher Scientific, Inc.). This reconstruction algorithm is optimized for processing parallel ARXPS data binned into 16 angles and matching the detection range (22−78°) of Theta Probe instruments. The constraints for reconstructed profiles included restricting the elemental concentrations to physically meaningful values (0−100%) and limiting the maximum depth. The latter was set to be approximately twice the depth of the region that contained significant variations in elemental profiles. Each profile reconstruction was performed at least 20 times; the reported averaged profiles are representative of profiles obtained from individual simulations.

2.6.2. Sputter Depth Profiles. The destructive elemental depth profiles were acquired in a K-Alpha instrument using a beam of low-energy Ar ions (beam energy 200 eV, beam current 1 μA) rastered over an area of ca. 4 × 2 mm^2. The spectrometer was set to a "snapshot" mode at a pass energy of 150 eV (energy resolution ca. 1.3 eV), which recorded "snapshots" of 21 eV wide spectral windows into 128 detector channels. Samples were tilted 50° away from the analyzer axis to maximize surface sensitivity and depth resolution.

The sputter depth profiles were produced following the deconvolution procedure from ref 22, whereby the raw concentrations are corrected to account for the differences in EAL values of photoelectrons from different elements. An adjustment factor was also included to account for the sample tilt of 50°. The *estimated depth scale* for sputter profiles was calibrated against the ARXPS reconstructed profile for Ar/O_2-treated samples. In the reconstructed profile, the O 1s signal drops to 50% of its maximum value at ca. 2.5 nm. Accordingly, the depth at which the O 1s signal drops to 50% of its maximum in the sputter profile was set to 2.5 nm. The resulting estimate of the polystyrene sputter rate by Ar ions at 200 eV was ca. 1/30 nm/s.

Table 1. Calculated EAL Values for Electrons Produced by XPS and REELS

electron origin	calculated EAL (nm)
C 1s	3.35
O 1s	2.68
N 1s	3.04
F 1s	2.25
valence band (VB)	4.1
REELS, 500 eV	1.52
REELS, 250 eV	0.90

Table 2. Contact Angles and Surface Energies of Untreated and Plasma-Treated Polystyrene

	immediately after treatment		samples aged 28 days	
sample	water contact angle (deg)	surface energy (mJ/m^2)	water contact angle (deg)	surface energy (mJ/m^2)
untreated PS	93	40	93	40
Ar/N_2 plasma	42	58	55	48
Ar/O_2 plasma	24	64	62	46
Ar/SF_6 plasma	103	17	98	19

3. Results

3.1. Surface Energy. The contact angle (CA) measurements were performed on untreated polystyrene samples, on samples immediately after plasma treatment, and on samples stored ("aged") for 28 days (Table 2). The untreated polystyrene film is hydrophobic, with correspondingly high water CA and relatively low surface energy. No impurities could be detected in spectra of freshly spin-cast polystyrene films, confirming the high quality of the model PS samples chosen for this study (Figures SI1

(17) Hesse, R.; Chasse, T.; Szargan, R. *Fresenius' J. Anal. Chem.* **1999**, *365*, 48–54.
(18) France, R. M.; Short, R. D. *Langmuir* **1998**, *14*, 4827–4835.
(19) Scofield, J. H. *J. Electron Spectrosc. Relat. Phenom.* **1976**, *8*, 129–137.
(20) Jablonski, A.; Powell, C. J. *Surf. Sci. Rep.* **2002**, *47*, 35–91.
(21) Tanuma, S.; Powell, C. J.; Penn, D. R. *Surf. Interface Anal.* **1994**, *21*, 165–176.
(22) Briggs, D.; Seah, M. P. *Practical surface analysis*; Wiley: Chichester, UK, 1992.
(23) Tougaard, S. *J. Vac. Sci. Technol., A* **2003**, *21*, 1081–1086.
(24) Paynter, R. W. *J. Electron Spectrosc. Relat. Phenom.* **2009**, *169*, 1–9.
(25) Cumpson, P. J. *J. Electron Spectrosc. Relat. Phenom.* **1995**, *73*, 25–52.
(26) Petrovykh, D. Y.; Kimura-Suda, H.; Tarlov, M. J.; Whitman, L. J. *Langmuir* **2004**, *20*, 429–440.

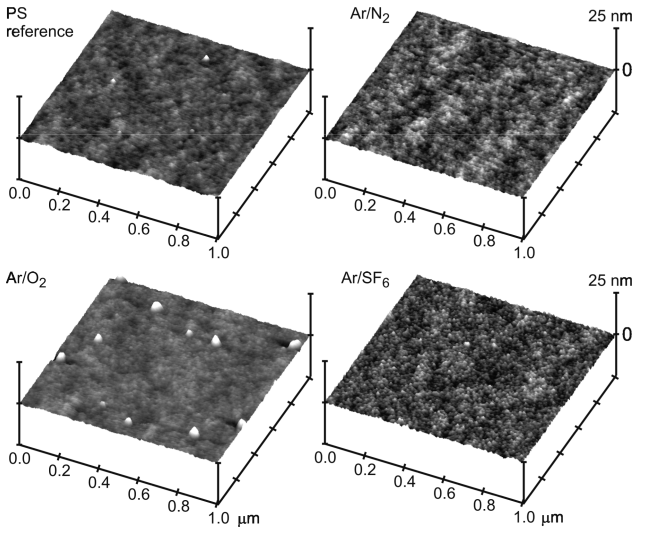

Figure 1. AFM images for untreated and Ar/N_2, Ar/O_2, and Ar/SF_6 plasma-treated polystyrene.

and SI2 in the Supporting Information). Immediately after Ar/O_2 and Ar/N_2 plasma treatments, polystyrene surfaces became hydrophilic, more hydrophilic after Ar/O_2 than after Ar/N_2. These treated surfaces, however, underwent hydrophobic recovery, as reflected in increasing water CA and decreasing surface energy over time. Moreover, after aging for 28 days, the surface energies became nearly identical for samples treated in Ar/O_2 and Ar/N_2 plasmas; further aging did not result in significant changes in surface energies. In contrast, after Ar/SF_6 treatment, the surface energy of polystyrene was reduced by approximately a factor of 2 and changed only minimally over time. XPS analysis described in the following sections was performed on the aged plasma-treated samples, because of their stable surface properties.

3.2. Surface Morphology. The surface roughness of polystyrene did not increase significantly after Ar/N_2 and Ar/O_2 plasma treatments (Figure 1). Root-mean-square (rms) roughness over $1 \times 1\ \mu m^2$ areas increased from 0.294 nm of the untreated polystyrene to 0.316, 0.436, and 0.447 nm after Ar/N_2, Ar/O_2, and Ar/SF_6 treatments, respectively. Power spectral densities (PSDs) were calculated for all samples. The PSD profiles (Figure SI3, Supporting Information) confirm that Ar/N_2 treatment produced only minimal change in the polymer surface morphology. The modification after Ar/O_2 plasma treatment was more pronounced but qualitatively similar. The morphology changes after the most reactive Ar/SF_6 treatment were larger and different from those produced by the other two treatments, both qualitatively and quantitatively. Finally, we note that the polystyrene surface roughening did not introduce any apparent artifacts or systematic deviations into the interpretation and modeling of the angle-resolved XPS data.

3.3. Elemental Composition. Elemental analysis by XPS was performed on aged plasma-treated and untreated polystyrene samples, that is, after their chemical compositions have stabilized. An overview of elemental compositions for these aged samples is presented in XPS surveys (Figure 2); the compositions are quantified in Table 3 based on high-resolution elemental spectra.

The *untreated* polystyrene data in Table 3 are for a sample stored in the ambient for 28 days after spin-casting. As expected for a homopolymer, the untreated film contained mostly carbon (99.7 atomic %). The small amount of oxygen observed on untreated polystyrene was adsorbed on the surface of the sample, as confirmed by the angle-resolved spectra (Figure 2, inset): the O

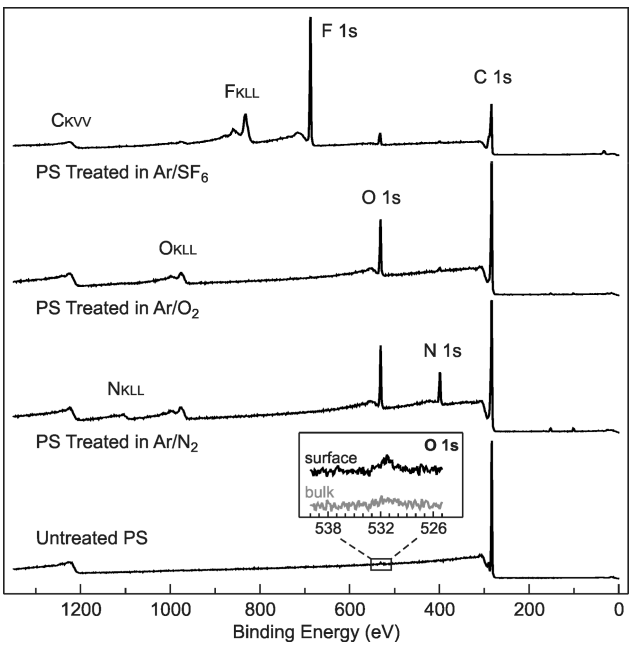

Figure 2. XPS surveys for aged plasma-treated and untreated polystyrene. Inset shows high-resolution angle-resolved data for the untreated PS in the O 1s region; ranges of photoelectron detection angles for "bulk" and "surface" spectra are 22−36° and 64−78°, respectively.

Table 3. Surface Composition of Aged Plasma-Treated and Untreated Polystyrene

	surface concentration (atomic %)			
element	untreated PS	Ar/O_2 plasma	Ar/N_2 plasma	Ar/SF_6 plasma
C	100	84.2	75.6	63.1
O	trace	15.8	13.1	5.1
N		trace	11.3	trace
F				31.8
Si[a]		trace	trace	

[a] Small Si signals represent dust particles produced by cleaving of silicon substrates.

1s peak is barely detectable in the bulk-dominated spectrum (ca. 9 nm sampling depth) but is more prominent in the surface-sensitive spectrum (ca. 3 nm sampling depth). The detected oxygen is thus incorporated in the adventitious contamination layer (water, OH groups, organic molecules) at the polymer surface rather than in the bulk of the polystyrene film. This conclusion is further supported by the absence of any detectable oxygen signal in XPS data from a fresh PS film (Figures SI1 and SI2 in the Supporting Information).

After treatment in Ar/O_2 plasma, primarily oxygen (15.8 atomic %) was incorporated into the polystyrene surface. In contrast, polystyrene surfaces treated in Ar/N_2 plasma contain comparable amounts of nitrogen (11.3 atomic %) and oxygen (13.1 atomic %). We note that the oxygen incorporation into the sample likely took place *after* the Ar/N_2 plasma treatment (as described in sections 3.6.1 and 4.2) rather than from any oxygen-containing impurities in the plasma or the bulk of the polystyrene film. The most significant modification of the elemental composition was produced by Ar/SF_6 plasma treatment, during which 31.8 atomic % of fluorine was incorporated into the surface.

3.4. Bulk Polymer Structure. The polymer structure below the plasma-modified surfaces was evaluated by obtaining spectra in the fingerprint VB region (Figure 3), which provides the

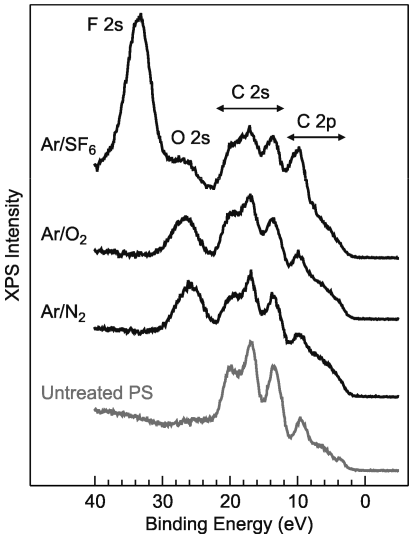

Figure 3. Valence band spectra of aged plasma-treated and untreated polystyrene.

Table 4. Assignments and BEs of VB Features for Polystyrene

sample	binding energy (eV)								
PS	20	17	13.6	9.9	6.4	3.9			
Ar/N_2	20	17	13.6	9.9			25	27	
Ar/O_2	20	17	13.6	9.9				27	
Ar/SF_6	20	17	13.6	9.9				27	34
label	A	B	C	D	E	F	G	H	I
element	C	C	C	C	C	C	N	O	F
orbital	2s	2s	2s	2s	pπ	pπ	2s	2s	2s

maximum sampling depth (ca. 12 nm) that can be achieved by conventional XPS without sputtering. The chemical structure of the polymer backbone produces characteristic VB features, which for polystyrene are remarkably similar to those of solid benzene.[27,28] The literature assignments of six characteristic VB features for benzene are summarized in Table 4: peaks A, B, C, and D ($2a_{1\,g}$, $2e_{1u}$, $2e_{2\,g}$, $2b_{1u}$) correspond to orbitals with strong C 2s character associated with C−C bonds, and peaks E ($1a_{2u}$ ($2b_1$)) and F ($1e_{1\,g}$($1a_2$, $1b_1$)) correspond to pπ molecular orbitals.[27,28] Molecular orbitals associated with the polyethylene skeleton broaden the peaks at BEs of 13.6 and 20 eV in polystyrene.[29] The polystyrene VB feature at BE $\approx$ 5 eV is missing in the VB spectrum of benzene, so it likely originates from C−H groups in the polymer backbone. The VB peak at BE = 3.9 eV is associated with the π orbitals that produce the shakeup satellite in C 1s core-level spectra of both polystyrene and benzene.

The plasma treatments did not completely transform the bulk polymer, as evidenced by the preserved major C 2s peaks in Figure 3. The peaks for the pπ orbitals are diminished, however, for all plasma-treated samples. In the VB of Ar/O_2-treated polystyrene, a new peak, assigned as O 2s, appears at BE = 27 eV. A similar feature, but asymmetric and with higher intensity, appears after Ar/N_2 treatment, suggesting assignment as an overlap of O 2s and N 2s peaks. After both Ar/O_2 and Ar/N_2 treatments, there is an increase in the peak intensity at BE = 9.9 eV and the slope for BE < 10 eV is also increased. Similar trends for plasma-treated polymers have been attributed to the O 2p character, occurring as lone pair electrons and in O 2p−H 1s and O 2p−C 2p molecular orbitals.[30,31]

After Ar/SF_6 treatment, a strong F 2s and a weaker O 2s peak appear in the VB region, in agreement with the surface composition changes observed in Figure 2 and Table 3. An F 2p peak also adds intensity to the C 2p envelope at BE = 10 eV. All the C 2s peak intensities are also increased by contributions from C−F bonds.[32] The increased slope for BE < 10 eV is similar to that observed after Ar/O_2 and Ar/N_2 treatments and may also include a F−F bond contribution at ca. 8 eV.[33]

3.5. C 1s Spectral Components. High-resolution ARXPS data in the C 1s region (Figure 4) were acquired to identify the presence and distribution of carbon-based functional groups in the aged plasma-treated samples (Table 5, Figure 5).

In the spectrum of *untreated* polystyrene (Figure 4a), the main peak at BE = 285.0 eV corresponds to carbon atoms in the aliphatic polymer backbone and phenyl rings. The presence of the latter is also confirmed by the π−π* shakeup (BE = 291.7 eV), which indicates unsaturated or aromatic carbon chemistry. Relative to the intensity of the main C 1s peak, the π−π* feature intensity remains at ca. 7% in angle-integrated as well as in bulk- and surface-dominated C 1s spectra (top, center, and bottom in Figure 4a, respectively). The constant relative intensity of the π−π* satellite indicates that the untreated polystyrene film is chemically uniform throughout the sampling depth of ARXPS measurements, that is, from the topmost 3 to 9 nm below the surface.

In contrast to the uniformly observable shakeup feature for untreated polystyrene, the π−π* satellites are reduced to < 2% of the total C 1s intensity after Ar/N_2 and Ar/O_2 treatments (Figure 5a and b), suggesting that phenyl rings are opened[36] and/or substituted[37] after plasma treatments. Furthermore, the π−π* relative concentration monotonically decreases from bulk- to surface-sensitive detection angles and becomes negligible in the most surface-sensitive spectra (Figure 5a and b), indicating that the Ar/N_2 and Ar/O_2 plasmas predominantly modify phenyl rings within the topmost 3 nm of the polymer surface. For the Ar/SF_6-treated sample, the CF_n components extend across the entire C 1s region (Figure 4d), masking any potential π−π* shakeup features. Accordingly, angle-resolved REELS measurements were added as a complementary evaluation of the presence and distribution of aromatic carbon in plasma-treated samples, as described in section 3.7.

All plasma treatments in this study produced qualitatively similar distributions of modified functional groups in polystyrene. In all treated samples, the relative concentrations of the C 1s components associated with unmodified polymer (C−C and π−π* features in Figure 5) decrease toward the surface of the polymer, reaching their minima (or even disappearing) in the topmost 3 nm of the film. In agreement with these trends of unmodified C 1s components, all the incorporated functionalities

(27) Riga, J.; Pireaux, J. J.; Caudano, R.; Verbist, J. J. *Phys. Scr.* **1977**, *16*, 346–350.
(28) Riga, J.; Pireaux, J. J.; Boutique, J. P.; Caudano, R.; Verbist, J. J.; Gobillon, Y. *Synth. Met.* **1981**, *4*, 99–112.
(29) Pireaux, J. J.; Riga, J.; Caudano, R.; Verbist, J. J.; Delhalle, J.; Delhalle, S.; Andre, J. M.; Gobillon, Y. *Phys. Scr.* **1977**, *16*, 329–338.
(30) Foerch, R.; Beamson, G.; Briggs, D. *Surf. Interface Anal.* **1991**, *17*, 842–846.
(31) Wells, R. K.; Badyal, J. P. S.; Drummond, I. W.; Robinson, K. S.; Street, F. J. *J. Adhes. Sci. Technol.* **1993**, *7*, 1129–1137.
(32) Endo, K.; Kaneda, Y.; Aida, M.; Chong, D. P. *J. Phys. Chem. Solids* **1995**, *56*, 1131–1140.
(33) Pireaux, J. J.; Riga, J.; Caudano, R.; Verbist, J. J.; Andre, J. M.; Delhalle, J.; Delhalle, S. *J. Electron Spectrosc. Relat. Phenom.* **1974**, *5*, 531–550.
(34) Wagner, C. D.; Riggs, W. M.; Davis, L. E.; Moulder, J. F.; Muilenberg, G. E. *Handbook of X-ray photoelectron spectroscopy*; Perkin-Elmer Corp.: Eden Prairie, MN, 1979.
(35) Beamson, G.; Briggs, D. *High resolution XPS of organic polymers: the Scienta ESCA 300 database*; John Wiley & Sons, Inc.: Chichester, 1992.
(36) Paynter, R. W. *Surf. Interface Anal.* **2002**, *33*, 14–22.
(37) Leggett, G. J.; Ratner, B. D.; Vickerman, J. C. *Surf. Interface Anal.* **1995**, *23*, 22–28.

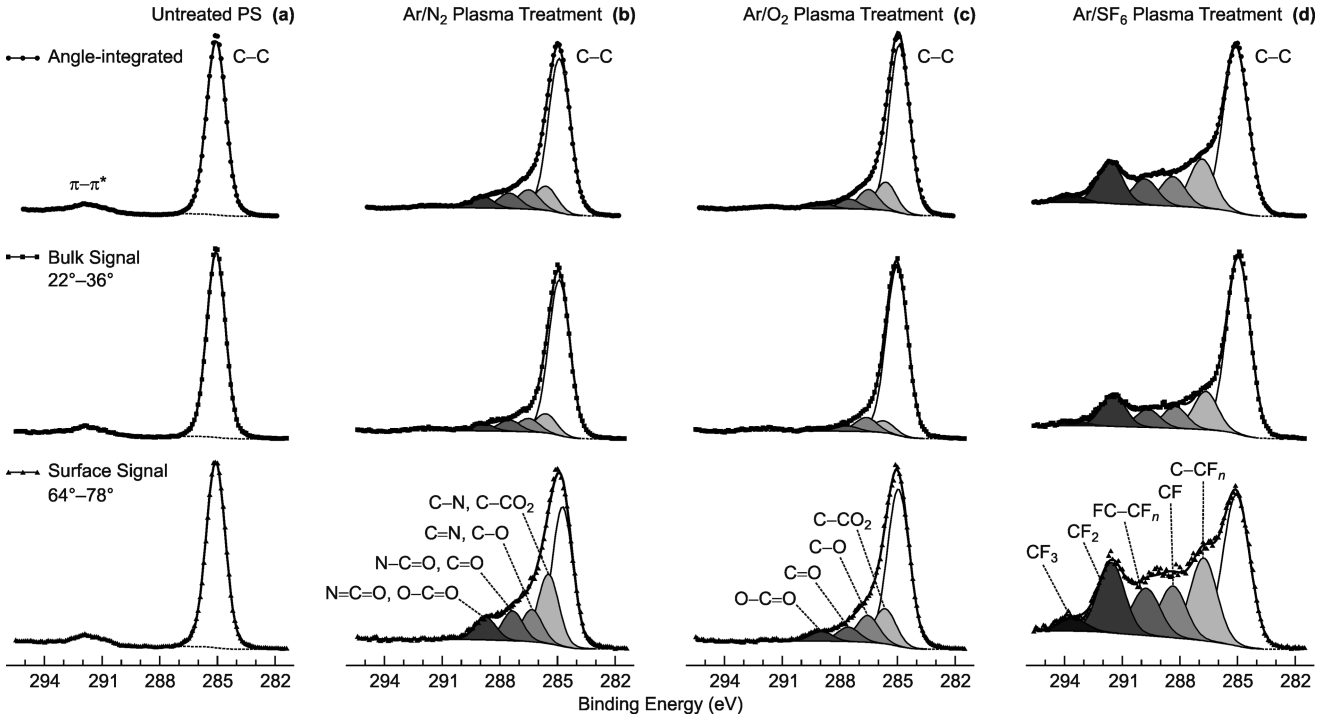

Figure 4. High-resolution C 1s spectra for aged plasma-treated and untreated polystyrene. Each panel shows ARXPS data for three ranges of photoelectron detection angles (top-to-bottom): angle-integrated (22−78°), bulk (22−36°, ca. 9 nm sampling depth), and surface-sensitive (64−78°, ca. 3 nm sampling depth). Symbols = data, thick lines = total fits, and thin lines = peak components and backgrounds. C 1s components characteristic of each treatment are indicated in the surface-sensitive spectra and listed in Table 5.

Table 5. Assignments of C 1s Components for Plasma-Treated Polystyrene

carbon chemistry[a]	BE (eV)	BE shift from C−C (eV)
C−C, C−H	285.0	
C−CO_2[b]	285.7	0.7
C−O (OH, C−O−C)	286.6	1.6 ± 0.2
C=O (−O−C−O−)	287.6	2.6 ± 0.2
O−C=O	289.0	4.0
$\pi-\pi^*$ shakeup	291.7	6.7
C−N	286.0	1.0
C=N	287.0	2.0
O=C−N	287.8	2.8
O=C=N	289.0	4.0
C−CF_n	286.6	1.6
CF	288.3	3.3
CF−CF_n	289.5	4.5
CF_2	291.2	6.2
CF_3	293.6	8.6

[a] Chemical assignments are based on refs 34 and 35. [b] β-shifted component was included in fits for plasma-treated polystyrene.

achieved their maxima in the spectra that sampled the topmost 3 nm of the film (Figures 4 and 5). For each treatment, the relative concentrations for most of the modified C 1s components decreased with their increasing BE (oxidation state of C), with the main notable exception being the CF_2 component after the Ar/SF_6 treatment.

The Ar/O_2-treated polystyrene exhibits C 1s components characteristic of single- and double-bonded C−O functionalities denoted as C−O, C=O, and O−C=O in Figures 4c, 5b and in Table 5 (β-shifted C−CO_2 was also included in the fits). The C−O functionality clearly dominates after the Ar/O_2 treatment, with a relative concentration that is higher than those of all the higher BE components throughout the film (Figure 5b).

The assignment and tracking of C 1s components is most challenging for the Ar/N_2-treated sample (Figure 4b), because C−CO_2/C−N, C=O/O=C−N, and O−C=O/O=C=N groups have overlapping BEs (Table 5). The relative concentrations of all single- and double-bonded C−O and C−N functionalities are within a factor of 2 of one another throughout the film (Figure 5a). The amine component, unfortunately, overlaps with the intense C−CO_2 peak, so the formation and distribution of amines could not be followed unambiguously.

The Ar/SF_6 plasma treatment resulted in incorporation of fluorinated groups including CF, CF_2, and CF_3 (Figures 4d, 5c and Table 5). Of all these components, the concentration of CF_2 was the highest at the surface and in the bulk, while that of CF_3 was the lowest (nearly an order of magnitude lower than the concentration of CF_2). The total concentration of the modified carbon groups was close to 50% near the polymer surface, indicating that the Ar/SF_6 plasma treatment provided the most efficient chemical modification of all the plasmas in this study.

3.6. Depth Profiles. The trends in Figure 5 suggest quasi-linear profiles for concentrations of carbon groups chemically modified by all the plasma treatments in this study. Such plots of raw ARXPS data, however, do not take full advantage of depth profiling by ARXPS. The surface sensitivity of XPS comes from exponential attenuation of photoelectrons defined by the "effective attenuation length" (EAL), which is known as λ in the standard XPS formalism.[20−22] The sampling depth (estimated as 3λ) shown in Figure 5 then provides only a coarse scale for depth profiling, because within that sampling volume the signal from the topmost layer dominates the spectrum but is convoluted with contributions from strong bulk peaks. More sophisticated models and methods can be used to extract additional structural information from ARXPS data.

Figures 6 and 7 show two types of depth profiles for plasma-treated polystyrene. The *nondestructive* depth profiles in Figure 6 were reconstructed based on parallel ARXPS data. The main

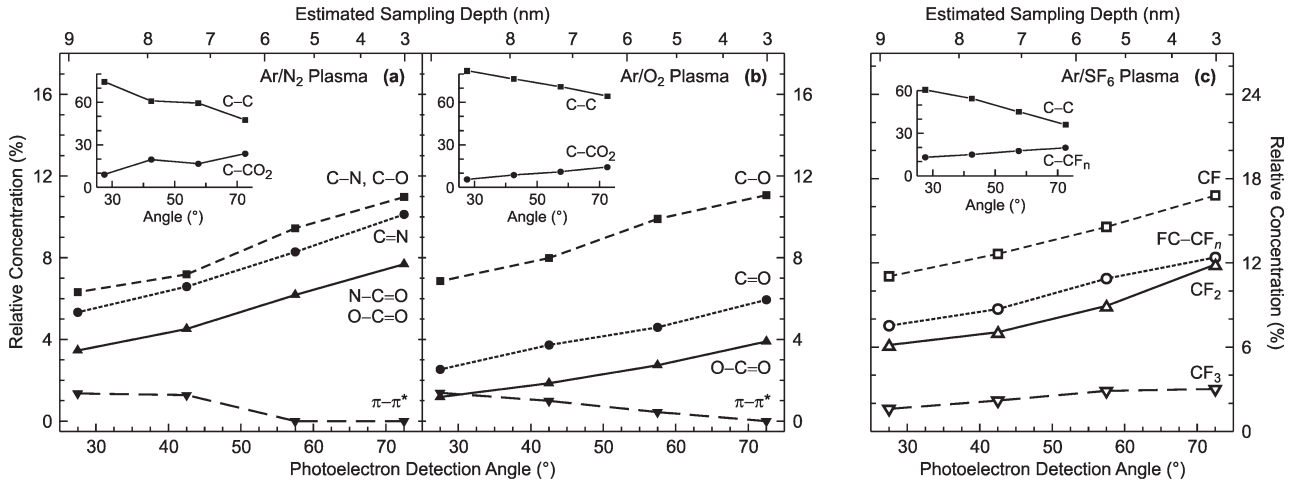

Figure 5. Depth distribution of functional groups in aged plasma-treated polystyrene. Relative concentrations of C 1s components observed in four ranges of photoelectron detection angles are shown for polystyrene treated in Ar/N_2 (a), Ar/O_2 (b), and Ar/SF_6 (c) plasmas. Insets show the data for the two highest intensity components in each panel. Assignments of C 1s components follow those in Figure 4 and Table 5.

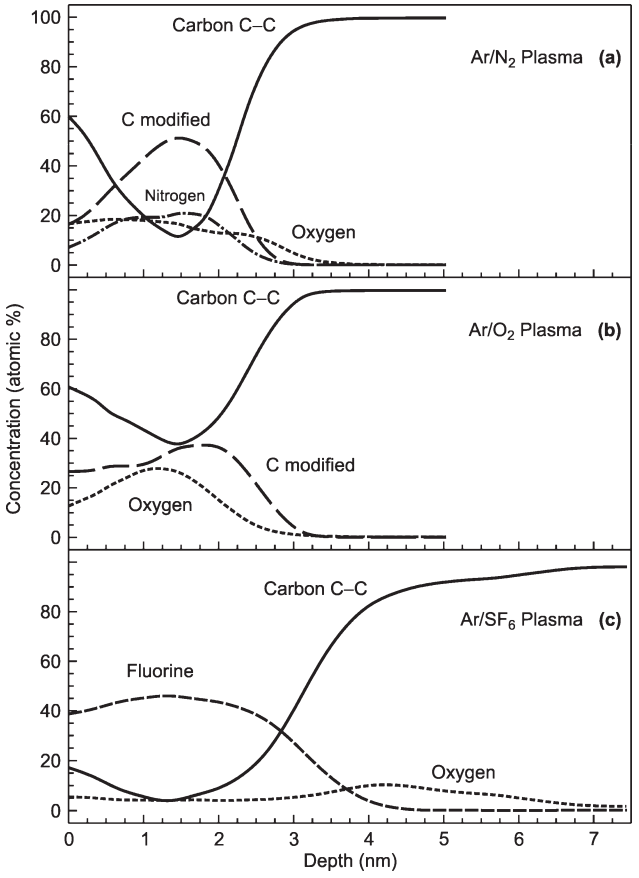

Figure 6. Nondestructive depth profiles for aged plasma-treated polystyrene. Relative concentrations of elements and chemical states of carbon in these profiles were reconstructed from parallel ARXPS data for Ar/N_2 (a), Ar/O_2 (b), and Ar/SF_6 (c) plasmas.

features of these nondestructive profiles were subsequently verified by *destructive* (sputter) depth profiles (Figure 7).

3.6.1. Nondestructive Depth Profiles. In contrast to traditional ARXPS measurements, whereby the detection angle is changed in discrete increments between 5 and 7 values,[22,25,36,38]

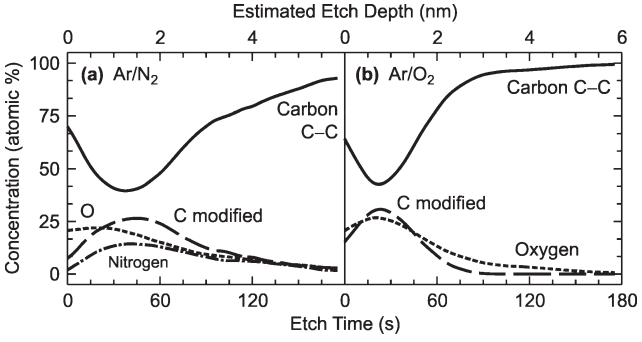

Figure 7. Sputtering depth profiles for aged plasma-treated polystyrene. Relative concentrations of elements and chemical states of carbon are shown for polystyrene treated in Ar/N_2 (a) and Ar/O_2 (b) plasmas. Sputtering was performed by a rastered beam of low energy (200 eV) Ar ions.

a Theta Probe instrument acquires ARXPS data sets over 16 or more angles in parallel, resulting in high signal-to-noise ratios and intrinsically minimal errors in normalizing the data. While still subject to the general constraints summarized in section 4.2.1, both quality and information content of these parallel ARXPS data sets are higher than those of traditional ARXPS data, thereby opening an opportunity to use a maximum-entropy algorithm[24] for reconstructing depth profiles (see sections 2.6.1 and 4.2.2 for details).

The most significant similarity between the profiles in Figure 6a and b is that the plasma modifications are limited to the topmost 3 nm of the polystyrene surface in both cases. An interface depth *was not* specified to constrain the maximum-entropy reconstruction for these profiles, so the shared maximum depth of modification is likely due to the underlying similarities between the effects of the two plasma environments on polystyrene surfaces. Furthermore, the distributions of the main elements from the respective plasmas are qualitatively similar: the N profile in Figure 6a and O profile in Figure 6b both feature a maximum located 1−2 nm below the surface and an approximately 50% decrease from the maximum toward the surface.

The O distribution in the Ar/N_2-treated sample is confined to the same overall depth as those of the main plasma elements in Figure 6a and b, but starts with a maximum at the surface and decreases roughly monotonically into the sample. This qualitative

(38) Haidopoulos, M.; Horgnies, M.; Mirabella, F.; Pireaux, J. J. *Plasma Processes Polym.* **2008**, *5*, 67–75.

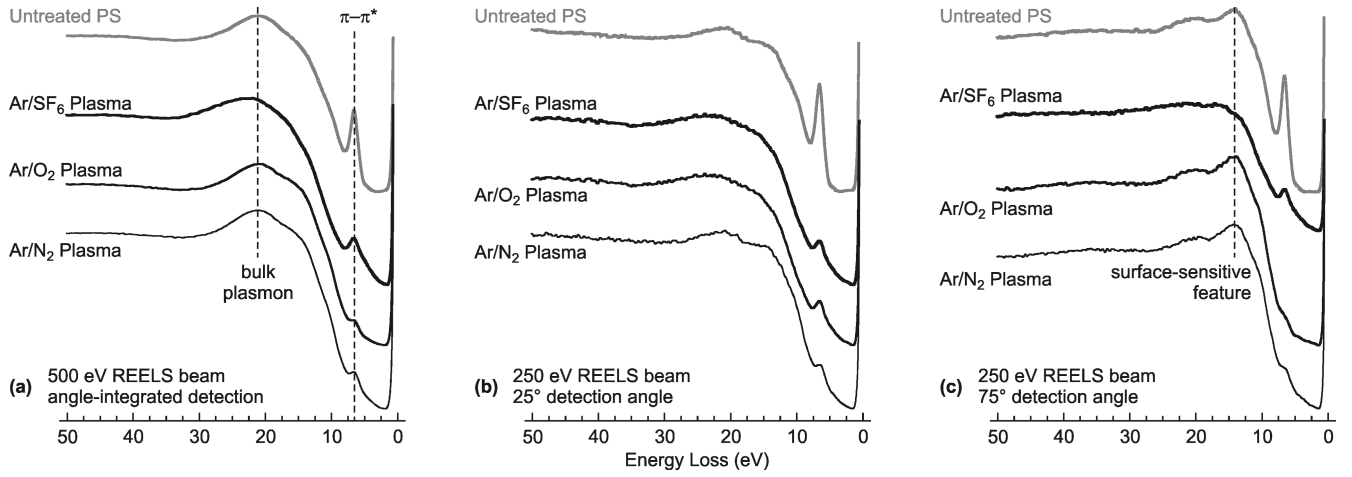

Figure 8. REELS data for aged plasma-treated and untreated polystyrene. Data in individual panels were obtained with beam energies of 500 eV (a) and 250 eV (b, c). Spectra in panel (a) are angle-integrated; spectra in panels (b) and (c) were acquired at bulk- (25°) and surface-sensitive (75°) detection angles.

difference suggests that some O incorporation occurred after the plasma-treated polystyrene surface was exposed to air. The monotonic O profile in Figure 6a also serves as a serendipitous internal control confirming that the peaked N and O distributions in Figure 6a and b are not simply artifacts produced by the reconstruction algorithm. The distributions of the modified C functionalities in Figure 6a and b essentially mirror those of the respective elements that provide the modification (O and N), a correlation that is consistent with the assignments and trends of functional groups in Figures 4 and 5.

The increase in the main C−C component toward the surface in Figure 6a and b is an intriguing common feature of both samples. The emergence of this feature in both C−C profiles highlights the type of structural information that cannot be discerned from the raw ARXPS data without additional reconstruction, primarily because the total C−C peak intensity is always dominated by the bulk signal for these samples. Detecting such an increase in the C−C concentration is particularly important for understanding the hydrophobic recovery behavior discussed in section 4.3.

The Ar/SF_6 plasma is expected to modify polystyrene surfaces more aggressively than do Ar/N_2 and Ar/O_2 plasmas, so the higher maximum depth of modification of 4 nm observed in Figure 6c is not surprising. The most interesting finding of the nondestructive depth profiling for the Ar/SF_6-treated sample in Figure 6c is the apparently "missing" profile for the chemically modified C component (analogous to those in Figure 6a and b). Multiple reconstructions were attempted assuming the presence of one or more $C-F_n$ functional groups, but the most reproducible reconstruction was obtained assuming just a single C−F group. The resulting concentration profile is not shown in Figure 6c because the algorithm accommodated the C−F constraint with a profile identical to that of the fluorine distribution. The coincidence of the reconstructed F and C−F profiles, of course, does not suggest that only C−F functionalities are present in the sample; the C 1s spectra in Figure 4 clearly indicate multiple types of $C-F_n$ functional groups. The identical reconstructed profiles for C−F and F simply indicate that the *average stoichiometry* of the F-modified polystyrene region is consistent with a 1:1 ratio of C to F atomic concentrations.

3.6.2. Destructive Depth Profiles. The sputter profiles in Figure 7 provide important independent confirmation of all the salient features observed in the reconstructed profiles from Figure 6. In particular, the peaked subsurface distributions of the main plasma-introduced elements are confirmed both qualitatively and quantitatively. The broad trailing tails of the depth profiles for O and N in Figure 7 are likely to result from knock-in effects, which are practically unavoidable in Ar sputtering of polymers.

The sputter profiles also captured the characteristic subsurface dip in the concentration of the C−C component, in excellent agreement with the reconstructed C−C profiles in Figure 6. All the profiles thus indicate a high concentration of the C−C component within the topmost 1 nm of the surface. Such a shallow layer, however, is beyond the depth resolution of the ARXPS data in Figure 4; therefore, a complementary REELS measurement was required to ascertain the corresponding carbon chemistry.

3.7. Angle-Resolved REELS. The REELS data collected for all four aged polymer surfaces provide a consistent and systematic comparison of the amount and distribution of saturated and unsaturated carbon functionalities (Figure 8).

The untreated polystyrene spectra in Figure 8 have a pronounced peak with energy loss of 21.4 eV, which corresponds to the bulk plasmon mode. The position of this feature is determined by the valence electron density and the electronic band structure of polystyrene.[39] The sharp peak at 6.6 eV is produced by interband $\pi-\pi^*$ transitions of benzene rings;[40] the degree of localization of these π-system states determines the width of the $\pi-\pi^*$ peak.[41]

The position of the bulk feature does not change after all the plasma treatments, indicating that the bulk structure of the polymer is largely preserved (in agreement with VB analysis in section 3.4). The reduced intensities of the $\pi-\pi^*$ peaks after plasma treatments, however, indicate that some of the benzene rings near the surface of the polymer are chemically modified by the plasmas. Remarkably, the Ar/SF_6 plasma that produces the most dramatic changes in carbon chemistry detected by XPS (in both C 1s and VB regions) results in the smallest removal of carbon unsaturation. In contrast, changes in both the bulk plasmon and $\pi-\pi^*$ peak have been reported previously for

(39) Marletta, G.; Pignataro, S.; Oliveri, C. *Nucl. Instrum. Methods Phys. Res., Sect. B* **1989**, *39*, 773–777.
(40) Ritsko, J. J.; Bigelow, R. W. *J. Chem. Phys.* **1978**, *69*, 4162–4170.
(41) Crecelius, G.; Fink, J.; Ritsko, J. J.; Stamm, M.; Freund, H. J.; Gonska, H. *Phys. Rev. B* **1983**, *28*, 1802–1808.

polystyrene bombarded by more energetic ions and electrons (at keV range energies), which were inferred to produce restructuring and graphitization of the polymer.[42−45]

The spectra in Figure 8a correspond to a sampling depth of ca. 4 nm, which is comparable to that of the most surface-sensitive ARXPS data in Figure 4. By lowering the electron energy, the sampling depth is reduced to ca. 2.4 and 0.7 nm for detection angles of 25° and 75° (Figure 8b,c), respectively (see section 2.5.5). An additional feature at ca. 14 eV emerges in the most surface-sensitive spectra for Ar/O_2 and Ar/N_2 plasma-treated polystyrene (Figure 8c). An analogous feature, however, does not appear for the fluorinated polystyrene, which also does not exhibit a strong bulk plasmon peak in Figure 8c. The small but persistent $\pi-\pi^*$ peaks in Figure 8c indicate that some level of carbon aromaticity is apparently present in the topmost 1 nm of all the polystyrene films aged in ambient air after the respective plasma treatments.

4. Discussion

The polystyrene surface modifications resulting from exposure to electron-beam-generated plasma in different gas environments are a direct result of the low ion energy and gas-phase chemistry that takes place. In molecular gas mixtures, the dominant reactions include electron−ion recombination, momentum transfer, and charge exchange reactions. For a given gas and plasma electron density, electron beams produce far fewer metastables and optically allowed states than do conventional discharges. Therefore, not only is the ion energy lower, but the number of UV and VUV photons emitted from the plasma is lower as well. We argue that these two effects account for the minimal modification of polystyrene surface morphology and the reduced depth of modification of the polystyrene, as shown in the sections below. Accordingly, the following discussion begins with an analysis of the surface properties: surface morphology, surface energy, and surface chemistry of the plasma-treated polystyrene. The mechanisms for the observed chemical modifications are discussed as well. The depth profiles of the plasma-modified polystyrene surfaces are analyzed and interpreted, to provide a common basis for comparing the modification depths reported in the literature for different plasma treatments of polymers. Finally, the apparent hydrophobic recovery of polystyrene surfaces treated by Ar/O_2 and Ar/N_2 plasmas is examined in detail, based on the complementary measurements of surface energy and chemistry.

4.1. Surface Properties of Plasma-Treated Polystyrene. *4.1.1. Surface Morphology.* In agreement with the anticipated minimal physical sputtering and ion-assisted chemical etching of polymer surfaces by electron-beam plasmas, the rms roughness was less than 1 nm for all treated polystyrene surfaces. The smallest roughness change (Figure 1 and Figure SI3 in the Supporting Information) was observed after the Ar/N_2 treatment, which was the least reactive gas mixture, whereas the largest uniform roughness increase occurred after the Ar/SF_6 treatment. This increased roughness was likely produced by chemical etching of the surface by reactive fluorine ions and atoms. The Ar/O_2 treatment produced low molecular weight (LMW) fragments, which were randomly distributed across the sample and contributed to the measured increase of surface roughness. It has been shown[46] that oxygen attachment to polymer chains makes the polymer more susceptible to chain scission and thus to formation of LMW species. However, it should be noted that the roughness of Ar/O_2-treated samples was much lower compared to that after discharge plasma treatment,[47] suggesting that electron-beam treatment results in less fragmentation and reduced loss of polymer chains from the surface.

The importance of polymer scission in the formation of LMW fragments is highlighted by comparing the AFM images of polystyrene after Ar/O_2 and Ar/SF_6 plasma treatments (Figure 1). The more reactive fluorine plasma might be expected to create more LMW aggregates than does the oxygen plasma. Extended Hückel molecular orbital (EHMO) calculations, however, predict fewer perturbations of the adjacent C atoms after F incorporation than after O incorporation,[48] meaning that PS should be less prone to scission after fluorination than after oxidation. The absence of visible LMW aggregates after Ar/SF_6 treatment (Figure 1) is consistent with this understanding of the mechanism that roughens O-treated but not F-treated PS surfaces.

4.1.2. Surface Energy and Chemistry. Although the ion energy bombarding the polymer surface was low, it was nevertheless sufficient to invoke significant changes in surface chemistry (Figure 2, Table 3) and surface energy (Table 2) of polystyrene. The surface energy of polystyrene exposed to Ar/SF_6 treatment decreased approximately two-fold due to incorporation of fluorine groups (CF, CF_2, and CF_3). The fluorine incorporation into the polystyrene surface likely started with hydrogen abstraction from the polymer backbone, accompanied by HF acid formation as a side product. Fluorine was then incorporated in the available radical centers. Remarkably, the surface energy of the Ar/SF_6-treated surface did not increase over time, as might be expected if oxygen from the ambient was incorporated after the plasma treatment. This might be due to saturated bonding configuration of the surface leaving few dangling bonds available, where oxygen could be directly connected to carbon. Furthermore, formation of F−O bonds is thermodynamically unfavorable,[49] and thus, polymers treated in Ar/SF_6 plasmas are less susceptible to fluorine removal via oxidation in air.

In contrast to the stability of the hydrophobic fluorinated surfaces, the Ar/O_2 and Ar/N_2 treatments produced, through incorporation of oxygen and nitrogen functionalities, hydrophilic polystyrene surfaces, for which hydrophobic recovery was observed over time (Table 2). The Ar/O_2 plasma introduced singly and doubly bonded C−O functionalities as well as some carboxyl groups (Figure 4c), which was very similar to the published results of RF plasma treatments,[36] suggesting a similar mechanism of plasma−surface interactions: hydrogen abstraction followed by oxygen substitution into the free radical sites. Volatile compounds including CO and CO_2 are formed as a result. However, the place of the hydrogen abstraction is under debate. Based on the thermal/photooxidative analysis, the preferred position of hydrogen abstraction in polystyrene is the tertiary C−H bond. In plasmas, however, hydrogen may be preferentially abstracted from benzene rings;[50] for example, phenol formation was suggested as the dominant reaction in oxygen plasmas.[51] The hydrogen substitution with oxygen is thermodynamically

(42) Compagnini, G.; Reitano, R.; Calcagno, L.; Marletta, G.; Foti, G. *Appl. Surf. Sci.* **1989**, *43*, 228–231.
(43) Marletta, G.; Catalano, S. M.; Pignataro, S. *Surf. Interface Anal.* **1990**, *16*, 407–411.
(44) Marletta, G. *Nucl. Instrum. Methods Phys. Res., Sect. B* **1990**, *46*, 295–305.
(45) Ujvari, T.; Toth, A.; Bertoti, I.; Nagy, P. M.; Juhasz, A. *Solid State Ionics* **2001**, *141*, 225–229.
(46) Hopkins, J.; Boyd, R. D.; Badyal, J. P. S. *J. Phys. Chem.* **1996**, *100*, 6755–6759.
(47) Jung, M.-H.; Choi, H.-S. *Thin Solid Films* **2006**, *515*, 2295–2302.
(48) Cain, S. R.; Egitto, F. D.; Emmi, F. *J. Vac. Sci. Technol., A* **1987**, *5*, 1578–1584.
(49) Egitto, F. D.; Matienzo, L. J.; Schreyer, H. B. *J. Vac. Sci. Technol., A* **1992**, *10*, 3060–3064.
(50) France, R. M.; Short, R. D. *J. Chem. Soc., Faraday Trans.* **1997**, *93*, 3173–3178.
(51) Moss, S. J.; Jolly, A. M.; Tighe, B. J. *Plasma Chem. Plasma Process.* **1986**, *6*, 401–416.

favorable because the C−H bond strength is lower than C−O and C═O (ester, ketones, aldehydes) bond strengths. It should be noted that, based on the EHMO calculations, the incorporation of oxygen weakens the polymer backbone by allowing not only for chain scission (and LMW formation discussed in the previous section) but also for migration of oxygen functionalities as discussed in section 4.3.

After Ar/N_2 treatments, the oxygen and nitrogen functionalities cannot be unambiguously distinguished in the C 1s spectra (Figure 4, Table 5). The observed ratios of the *total amounts* of the incorporated nitrogen and oxygen to carbon in the backbone, however, indicate that heterosubstituted carbon functionalities such as amides are created instead of pure nitrogen- and oxygen-based functional groups. This result is not surprising: exposure of plasma-treated polymers to air, especially when they are treated with inert gases such as argon[18,52] or nitrogen,[53,54] causes oxygen incorporation. When exposed to air, imines created during nitrogen treatment may be hydrolyzed.[54] The detailed analysis of nitrogen depth profiles (Figures 6 and 7) in section 4.2.2 also confirms that oxygen incorporation most likely occurred via oxidation in air after Ar/N_2 treatment.

For all electron-beam plasma treatments, the concentration of incorporated groups specific to the certain environment was the highest in the topmost 3 nm of the polymer surfaces (Figures 5 and 6). The trends observed for the $\pi-\pi^*$ features in XPS and REELS data consistently indicate that in plasma modification reactions, benzene rings are favored over the polyethylene backbone. The $\pi-\pi^*$ features characteristic of unsaturated benzene rings present in unmodified polystyrene are clearly diminished after all plasma treatments (Figures 3, 4, and 8). In agreement with the distribution of the plasma-modified groups, the modification of benzene rings via substitution reactions was observed predominantly in the topmost 3 nm of polystyrene.

4.2. Depth Profiles. The lack of a standard convention for reporting the modification depths estimated from ARXPS data leads to a certain degree of confusion about the values appearing in the literature. Different models used for interpretation of ARXPS data actually produce different estimates of the plasma penetration depths, even for the same sample.[36,38] An accurate comparison between the plasma modification mechanisms of different plasma sources therefore requires a careful examination and comparison of the respective reported depth profiles and characteristic values for penetration depths highlighted in different papers.

4.2.1. General Features of ARXPS Depth Profiling. A depth profile *reconstruction* based on ARXPS data, mathematically, is an ill-posed inversion problem.[24,25] The resulting sensitivity of reconstruction algorithms to noise in the experimental data necessarily limits the details and features of depth profiles that can be unambiguously reconstructed from any given data set.[25] Specifically, the limited information content of any practical ARXPS data set imposes a tradeoff between composition uncertainty and depth resolution in a depth profile that can be recovered by *any algorithm*.[25] In practice, this tradeoff is optimally resolved by matching the complexity of the recovered concentration profile to the quality and information content of the underlying ARXPS data set. In order of increasing complexity, three standard models used for depth profile reconstruction of plasma-treated polymers are a two-point boxcar, a three-point trapezoid, and a four-point model proposed by Cumpson (Scheme 1).[24,25,36]

Scheme 1. Three Model Depth Profiles for Interpretation of ARXPS Data: Boxcar, Trapezoid, and Cumpson

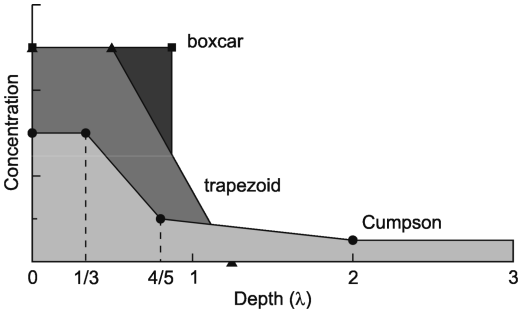

The boxcar model assumes a constant concentration in the surface layer and a sharp interface between the surface layer and bulk (Scheme 1). Except for special samples, these assumptions are not generally correct, but they result in *underestimating* the depth of the actual concentration profile, because the concentration is artificially fixed at its elevated "surface" value within a respectively shallow region.

The additional control points in the trapezoid and Cumpson profiles allow the reconstructions to relax away from an unrealistically constrained boxcar profile (Scheme 1). This relaxation typically extends the reconstructed profile deeper into the sample than the boxcar estimate, because the boxcar model is essentially designed to estimate an upper limit of the concentration. The concentration values calculated at additional points of the more sophisticated models tend to be lower than the boxcar estimate and hence spread deeper into the sample, because the area under the properly reconstructed profiles remains approximately constant (the "amount of substance"[23] is conserved) (Scheme 1). In the boxcar and trapezoid models, the positions of the control points are calculated, whereas in the Cumpson model the control points are fixed at $1/3\lambda$, $4/5\lambda$, and 2λ, thereby virtually ensuring that the reconstructed profile will show variable concentration across the topmost 2λ of the sample (and constant concentration below 2λ).[25]

4.2.2. Depth Profile Analysis. The profiles in Figure 6 were reconstructed using a *maximum-entropy algorithm* that has been optimized for processing parallel ARXPS data binned into 16 angles and matching the detection range of a Theta Probe instrument. Unlike the simpler models (boxcar, trapezoidal, and Cumpson in Scheme 1), the maximum-entropy method does not assume a particular shape of a depth profile but rather includes a *regularization procedure*, which ensures that the reconstructed depth profiles are not too detailed (or variable) and thus unrealistic.[24,25] The reconstructed profiles in Figure 6 reveal important details about the depth distributions of elements, including those introduced *during* and *after* plasma treatments.

Oxygen distributions in Figure 6, in particular, reflect the different incorporation mechanisms for PS treated in different plasma environments. Whereas the Ar/O_2 plasma is expected to incorporate oxygen into PS, the Ar/N_2 and Ar/SF_6 plasmas are not expected to oxidize PS directly, as neither these environments nor the bulk PS film contain any significant amount of oxygen. Nevertheless, after aging in air for 28 days, clear oxygen signals are observed from both Ar/N_2- and Ar/SF_6-treated samples (Figure 2, Table 3).

We already noted in section 4.1.2 that exposure of plasma-treated polymers to air is known to cause oxygen incorporation,[18,52−54] primarily into free radicals or strained rings at the

(52) Lock, E. H.; Walton, S. G.; Fernsler, R. F. *Plasma Processes Polym*. **2009**, *6*, 234–245.
(53) Sanchis, M. R.; Calvo, O.; Fenollar, O.; Garcia, D.; Balart, R. *Polym. Test*. **2008**, *27*, 75–83.
(54) Foerch, R.; McIntyre, N. S.; Sodhi, R. N. S.; Hunter, D. H. *J. Appl. Polym. Sci*. **1990**, *40*, 1903–1915.

surface. As expected, this type of oxygen incorporation is most evident after plasma treatment in a relatively inert Ar/N_2 environment, whereby the aged plasma-treated PS contains more oxygen than nitrogen at the surface (Figure 6a). The oxygen distribution in this sample is maximized at the surface (in contrast to the subsurface maximum of the nitrogen distribution) and monotonically decays with depth; both of these characteristics suggest a mechanism that involves diffusion of oxygen from the surface. Furthermore, post-treatment oxygen incorporation can proceed into sites damaged but not modified by the plasma, so the distribution of oxygen can be deeper than that of the primary plasma elements, as indeed is observed in Figure 6a and c. The Ar/SF_6 plasma, apparently, did not leave as many dangling bonds in the modified region as did the less reactive Ar/N_2 plasma, so in Figure 6c oxygen incorporation is seen immediately below the fluorinated region, that is, in the region where PS was not modified by the plasma treatment.

4.2.3. Depth of Surface Modification. The most important feature in Figures 6 and 7 is the low total depth of plasma modification: ca. 3 nm for Ar/O_2 and Ar/N_2 plasmas and ca. 4 nm for Ar/SF_6 plasma, both of which are roughly half the modification depth discussed below for RF discharges (refs 36 and 38).

In order to illustrate the differences between the electron-beam and the RF plasma treatments, our Ar/O_2 depth profiles were compared with ARXPS depth profiles of RF plasma-treated polystyrene in Ar/O_2 environment (10% oxygen in the mixture) using low RF powers (< 20 W), high pressures (> 100 mTorr) and the same treatment time (30 sec).[36,38] It should be noted that fewer detection angles (6 and 5, respectively) and thus the simpler model profiles were used to interpret the ARXPS data for RF-plasma-treated samples: boxcar and Cumpson in both refs 36 and 38, as well as trapezoid in ref 36. As discussed in section 4.2.1., the boxcar model is expected to provide the lowest possible estimate of the maximum modification depth, so the boxcar depths as low as 3 nm for the O distributions in refs 36 and 38 are significantly *underestimating* the actual modification depths. The extent of this underestimation is demonstrated by the Cumpson profiles, which for the same samples show O concentrations extending considerably deeper than 3 nm.[36,38] Because plasma modification is highly unlikely to generate the uniform O profile with a sharp cutoff at the trailing edge, as assumed in the boxcar model, the more flexible Cumpson model should provide a more realistic assessment of the concentration profiles for plasma-treated samples. While the depths at which concentration is evaluated are fixed in the Cumpson model,[25] the positions of those reference points allow comparison of the resulting O profiles from refs 36 and 38 to that in Figure 6b.

The O profiles reported in ref 38 are qualitatively similar to that in Figure 6b: they also exhibit a maximum below the surface and a gradual decrease of O concentration toward the surface and the bulk. The maximum O concentration, however, is located close to 3 nm below the surface for RF-plasma-treated samples, in contrast to ca. 1.3 nm in Figure 6b. The decrease in O concentration toward the surface and bulk is also steeper for the sample in Figure 6b, for which a drop of ca. 50% occurs toward the surface and a comparable distance into the bulk, whereas for RF-plasma-treated samples the concentration change is only ca. 30% and over about twice the range of depth. The O profile in Figure 6b is thus *quantitatively* both narrower and closer to the surface than those reported in ref 38.

The O profiles in ref 36 are only reported for relatively fresh samples (aged less than 4 days), so they are not directly comparable to the profile in Figure 6b. Qualitatively, the O profiles in ref 36 are similar to those for freshly oxidized samples in ref 38, exhibiting a maximum at the surface and a concentration drop within the top 3 nm. The O profiles for samples freshly oxidized in RF plasmas, however, consistently indicate 5−10% concentration of O at 6 nm depth,[36,38] which in the context of the Cumpson model indicates that the maximum depth of modification is > 6 nm in Ar/O_2 RF plasmas, in contrast to ca. 3 nm total modification depth produced by the electron-beam plasma.

A careful examination of the RF treatment parameters in refs 36 and 38 reveals that low RF powers and high pressures would result in the formation of thick collisional sheaths and thus in ion energies that are comparable with the ones measured in electron-beam-produced plasma. Moreover, the use of low RF power and high pressure would result in lower plasma density yet high dissociation rates, leading to large radical and excited species production rates. Thus, one would expect large photon fluxes relative to the ion flux. It has been shown that UV and VUV photons affect the polymer surface modification process not only in noble gases (CASING)[6] and relatively inert gases (nitrogen and hydrogen) but also in oxygen and fluorine environments.[55,56]

4.3. Hydrophobic Recovery. The gradual decrease of the surface energy with aging is well documented for plasma-treated polymers.[38,52] Two possible mechanisms, one intrinsic and one extrinsic, have been proposed in the literature. The intrinsic hydrophobic recovery can be produced by reorientation or diffusion of polar groups away from the plasma-treated surface and toward the bulk of a hydrophobic polymer.[57] For such polymers, the migration of polar groups toward the bulk is a thermodynamic phenomenon driven by the minimization of their surface free energy.[58] The extrinsic mechanism relies on adsorption of hydrophobic (aliphatic) molecules from air onto the reactive plasma-modified polymer surfaces.[59]

While the typical contact angle and XPS measurements can readily detect that a hydrophobic recovery has occurred, the characteristic signatures that can be predicted by the two proposed mechanisms are not easy to distinguish experimentally. For example, increased water CA values would be expected from both models, as indicated by the "hydrophobic recovery" moniker. For an intrinsically aromatic polymer, such as polystyrene, the main possible distinction between the intrinsic and extrinsic mechanisms of hydrophobic recovery is that the former should produce a layer of unmodified *aromatic* carbon at the surface, whereas the latter should deposit a layer of *aliphatic* carbon. Conventional XPS analysis will not be able to distinguish between these two types of surface carbon layers, but the detailed ARXPS and REELS data in this study provide a unique opportunity to resolve the ambiguity.

Indirect evidence from the ARXPS and REELS data for untreated polystyrene (Figures 4a and 8) argues against significant accumulation of adventitious hydrocarbons on polystyrene surfaces. While a *hydrophobic* polystyrene surface can be expected to promote the putative accumulation of aliphatic hydrocarbons, the nearly constant intensity of $\pi-\pi^*$ (i.e., unsaturated carbon) features in angle-resolved XPS and REELS data clearly indicate that any such accumulation of saturated hydrocarbons is

(55) Wertheimer, M. R.; Fozza, A. C.; Hollander, A. *Nucl. Instrum. Methods Phys. Res., Sect. B* **1999**, *151*, 65–75.
(56) Corbin, G. A.; Cohen, R. E.; Baddour, R. F. *Macromolecules* **1985**, *18*, 98–103.
(57) Zekonyte, J.; Zaporojtchenko, V.; Faupel, F. *Nucl. Instrum. Methods Phys. Res., Sect. B* **2005**, *236*, 241–248.
(58) Murakami, T.; Kuroda, S.; Osawa, Z. *J. Colloid Interface Sci.* **1998**, *200*, 192–194.
(59) Davidson, M. R.; Mitchell, S. A.; Bradley, R. H. *Surf. Sci.* **2005**, *581*, 169–177.

minimal. The *hydrophilic* plasma-treated polystyrene surfaces will be less attractive for hydrophobic adventitious molecules, so an accumulation of enough hydrocarbons to induce hydrophobic recovery is unlikely on polystyrene surfaces treated by Ar/N_2 and Ar/O_2 plasmas.

The above indirect evidence is further supported by the behavior of $\pi-\pi^*$ features in REELS data for polystyrene surfaces treated by Ar/N_2 and Ar/O_2 plasmas (Figure 8). The $\pi-\pi^*$ peaks are suppressed but not completely eliminated after plasma treatments. Moreover, the $\pi-\pi^*$ peaks retain some intensity in REELS data from the topmost 1 nm of these polymers (Figure 8c), indicating an aromatic character of the topmost carbon layer, which is inconsistent with a putative accumulation of adventitious aliphatic hydrocarbons.

The *direct evidence* for the intrinsic mechanism comes from the depth profiles in Figures 6a,b and 7. The consistent increase in hydrophobic C−C carbon in the topmost 1 nm of these films and the concomitant shift of the modified C concentration below 1 nm are exactly the signatures one would expect from reorientation or diffusion of polar C groups toward the bulk. Significantly, the preceding discussion clearly indicates that the topmost 1 nm of these films *is not* dominated by aliphatic hydrocarbons, so the carbon enrichment observed in Figures 6 and 7 can be produced only by reorientation/diffusion of undamaged aromatic polymer fragments from the bulk and not by contamination. The intrinsic mechanism for hydrophobic recovery of plasma-treated polystyrene is also consistent with the evolution of oxygen profiles observed for freshly oxidized and aged polystyrene samples in previous studies.[36,38]

5. Conclusions

In this study, polystyrene was subjected to electron-beam-generated plasmas produced in mixtures of Ar/O_2, Ar/N_2, and Ar/SF_6. The plasma-induced changes were examined using a suite of complementary analytical techniques after roughly a month of aging. Regardless of gas background, plasma treatments produced a significant change in surface chemistry without significantly changing the surface morphology. Specifically, O, N, and F functional groups were introduced using mixtures containing O_2, N_2, and SF_6, respectively, while the increase in rms surface roughness was less than 0.153 nm. Not surprisingly, the presence of O and N groups leads to a more hydrophilic surface, while F groups produce a more hydrophobic surface.

High-resolution, nondestructive and destructive depth profiles show all functional groups were confined to the topmost 3−4 nm of the polymer surface and that the polymer structure was preserved below 9 nm. The unambiguous observation of a carbon-rich layer with aromatic chemistry within the top 1 nm of the surface indicates that it was produced by reorientation/diffusion of undamaged aromatic polymer fragments from the bulk during hydrophobic recovery and not by contamination.

The shallow modification depth, which is almost a factor of 2 lower than the modification depths produced by RF plasmas, and the minimal plasma-induced surface roughening are linked to the unique properties of electron-beam-generated plasmas. Unlike most plasma discharges, these plasmas are characterized by a combination of low incident ion energies and relatively low fluxes of photons and radicals compared to the ion flux This combination of features indicates that electron-beam-generated plasmas are well-suited for applications requiring chemical functionalization without significant changes in surface morphology, such as the case when nanometer scale thickness or surface features of polymers must be preserved.

Acknowledgment. E.H.L. was an NRL/NRC Postdoctoral Research Associate when this work was performed. The work at NRL was funded by the Office of Naval Research. D.Y.P. also received support from the Air Force Office of Scientific Research.

Supporting Information Available: XPS survey of a freshly spin-cast PS film; high-resolution XPS data for a freshly spin-cast PS film; power spectra of surface roughness for plasma-treated PS films. This material is available free of charge via the Internet at http://pubs.acs.org.

Supporting Information

Surface Composition, Chemistry, and Structure of Polystyrene Modified by Electron-Beam-Generated Plasma

Evgeniya H. Lock,[*,#] Dmitri Y. Petrovykh,[&,†] Paul Mack,[‡] Tim Carney,[‡] Richard G. White,[‡] Scott G. Walton,[#] Richard F. Fernsler[#]

[#]*Plasma Physics Division, Naval Research Laboratory, Washington, D.C. 20375;* [&]*Chemistry Division, Naval Research Laboratory, Washington, D.C. 20375;* [†]*Department of Physics, University of Maryland, College Park, MD 20742;* [‡]*Thermo Fisher Scientific, The Birches Industrial Estate, Imberhorne Lane, East Grinstead, West Sussex, RH19 1UB, UK*

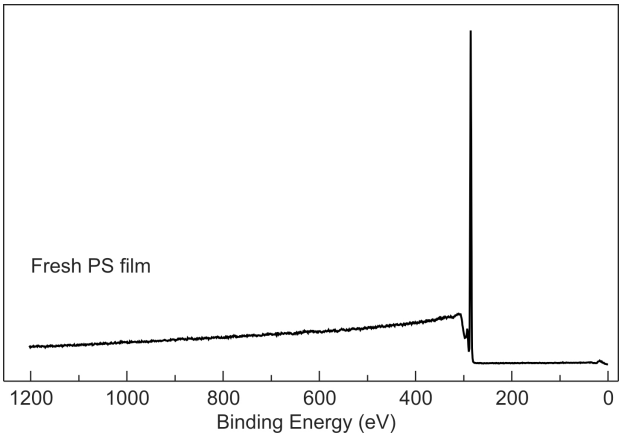

Figure SI1. XPS survey of a freshly spin-cast polystyrene film.

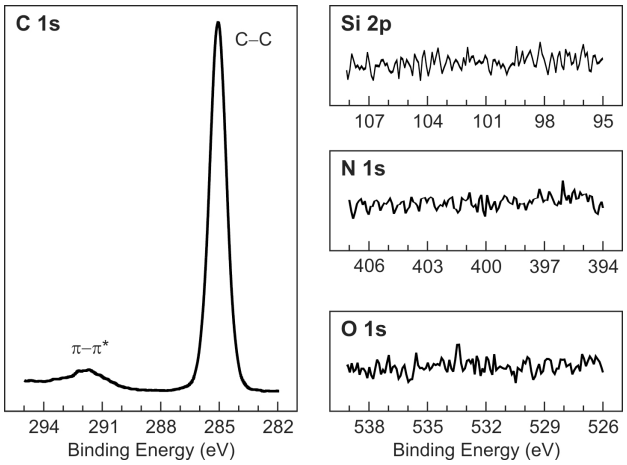

Figure SI2. High-resolution XPS data for a freshly spin-cast polystyrene film. Note that any O, N, or Si impurities or contaminants are below XPS detection limit for these PS films.

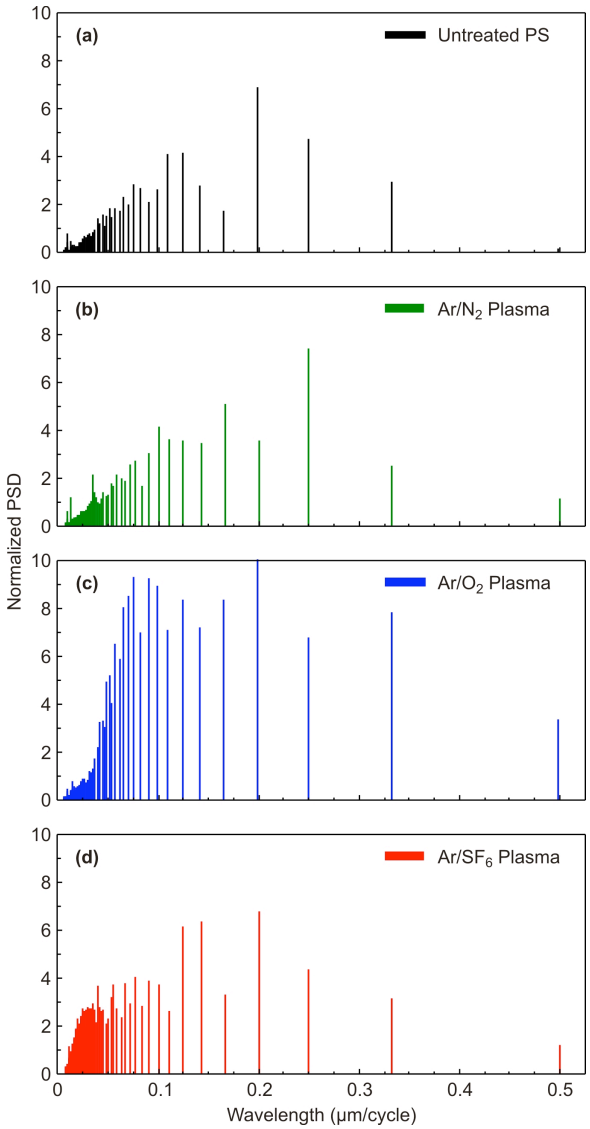

Figure SI3. Power spectra of surface roughness for plasma-treated polystyrene films. PSD profiles were calculated from AFM data (Figure 1) for PS surfaces treated in Ar/N_2 (b), Ar/O_2 (c), and Ar/SF_6 (d) plasma environments. Panel (a) shows a reference PSD for untreated PS sample.

[*]Author to whom correspondence should be addressed: Evgeniya H. Lock, Plasma Physics Division, Naval Research Laboratory, Washington DC 20375
E-mail: evgeniya.lock@nrl.navy.mil; Phone: 202-767-0351; Fax: 202-767-3553.